Journal of Engineering Physics and Thermophysics, Vol. 83, No. 5, 2010

STUDY ON THE HEAT-TRANSFER CHARACTERISTICS AND PRESSURE DROP IN CHANNELS WITH ARC-SHAPED WAVY PLATES

Naphon Paisarn

UDC 536.24

The heat-transfer characteristics and pressure drop in a channel with arc-shaped wavy plates are presented. The test channel with two opposite wavy plates, whose peaks are in-phase or out-of-phase, are tested under constant wall heat flux conditions. The experiments are made for the Reynolds number and heat flux in the ranges 1500–2500 and 0.5–1.2 kW/m^2, respectively. The effects of relevant parameters on the heat-transfer characteristics are considered. A turbulent mathematical model is employed to simulate the temperature and velocity distributions. The predicted results are verified by comparing with measured data, and reasonable agreement is obtained. Due to the onset and growth of the recirculation zones, the convective heat transfer in the channel with wavy plates is higher than that with flat plates.

Keywords: *heat-transfer enhancement, arc-shaped wavy plate.*

Introduction. A fluid flowing through a channel with wavy surfaces has a significant effect on the enhancement of heat transfer due to the breaking and destabilization of the thermal boundary layer. Therefore, using wavy plates is a suitable method to improve the thermal performance in designing heat exchangers. The heat transfer and flow characteristics in the channel with wavy plates have been widely studied previously. Sunden and Skoldheden [1, 2] experimentally and numerically considered the heat transfer and pressure drop in corrugated channels and smooth tubes under a constant heat flux. Sawyer et al. [3] numerically and experimentally studied the effect of three-dimensional hydrodynamics on the enhancement of heat transfer in corrugated channels. Bereiziat and Devienne [4] experimentally studied the flow characteristics of Newtonian and non-Newtonian fluids in a corrugated channel. Fabbri [5, 6] investigated laminar convective heat transfer in a channel with smooth and corrugated walls. Mehrabian and Poulter [7] considered the effect of the corrugation angle on the performance of a flow between two identical APV SR3 plates. Gradeck and Lebouche [8, 9] observed flow patterns of a gas-liquid flow and analyzed heat transfer in horizontal corrugated channels by using nitrogen and water as working fluids. Vasudevaiah and Balamurugan [10] adopted the transport equation to study convective heat transfer in a corrugated microchannel. Zimmerer et al. [11] considered the effects of the inclination angle, wavelength, amplitude, and shape of the corrugation on heat and mass transfer in a heat exchanger. Wang and Chen [12] applied a simple coordinate transformation method and the spline alternating-direction implicit method to determine the heat-transfer rates. Effects of the wavy geometry, Reynolds number, and Prandtl number on the skin friction and Nusselt number were considered. Hamza et al. [13] experimentally studied the effects of the operating parameters on laminar flow forced-convection heat transfer in air flowing in a channel having a V-corrugated upper plate. Metwally and Manglik [14] simulated laminar periodically developed forced convection in sinusoidal corrugated-plate channels by the control volume finite-difference method. Islamoglu and Parmaksizoglu [15–17] numerically and experimentally studied the effect of the channel height on the enhancement of the heat-transfer characteristics in a corrugated heat-exchanger channel. In addition, artificial networks were employed to analyze the heat transfer in corrugated channels. Naphon [18–20] studied the heat-transfer characteristics and pressure drop in a corrugated channel with different V-shaped wavy plates and channel heights. Kuhn and Rohr [21] employed digital particle image velocimetry and planar laser-induced fluorescence techniques to examine the spatial variation of the streamwise and normal velocity components at the heated wavy surface.

Department of Mechanical Engineering, Faculty of Engineering, Srinakharinwirot University, 63 Rangsit-Nakhornnayok Rd., Ongkharak, Nakhorn-Nayok, 26120, Thailand; email: paisarnn@swu.ac.th. Published in Inzhenerno-Fizicheskii Zhurnal, Vol. 83, pp. 995–1003, September–October, 2010. Original article submitted December 2, 2008; revision submitted October 5, 2009.

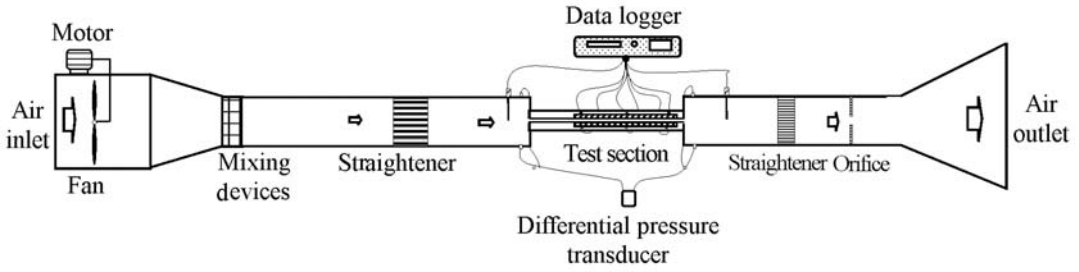

Fig. 1. Schematic diagram of experimental apparatus.

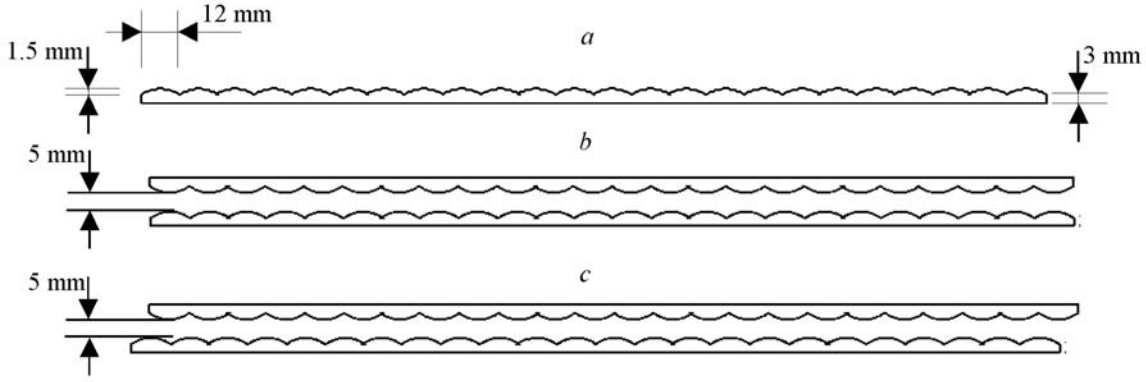

Fig. 2. Schematic diagram of the arc-shaped wavy plates: dimensions (a); in-phase (b) and out-of-phase (c) arrangements.

As is seen from the above survey, numerous experimental and theoretical studies have been reported on heat transfer and pressure drop on a corrugated surface with various configurations. However, only a few of these works were devoted to the heat-transfer characteristics and pressure drop in a channel with two opposite arc-shaped wavy plates. The objective of this paper is to study these characteristics in such a channel, where the peaks have in-phase and out-of-phase arrangements. The effects of various relevant parameters on the heat-transfer characteristics are considered.

Experimental Apparatus and Method. *Test Loop.* Figure 1 shows a schematic diagram of the experimental apparatus whose test loop consists of a test section, chilled air loop, and data acquisition system. The open-loop wind tunnel is a rectangular air duct fabricated from Acrylic of size 15 × 15 cm and length 295 cm. The duct is insulated with a 5-mm-thick Aeroflex standard sheet. Air in the open wind tunnel is discharged by an axial fan into the channel, passes through a mixing device, straightener, test section, and orifice, and then is discharged to the atmosphere. The orifice plate based on the ISO 5167 standard is employed to measure the air flow rate. The pressure drops across the test section and orifice plate are measured by a digital manometer with an accuracy of 0.02% of full scale. There are four pressure taps on each wall upstream and downstream of the test section and the orifice plate. All the T-type copper-constantan thermocouple probes with an accuracy of 0.1% of full scale which were precalibrated by the dry-block temperature calibrator with 0.01^{o}C precision are employed to measure the inlet and outlet air temperatures.

Test Sections. The arc-shaped wavy plates are presented in Fig. 2. Here, the arc size is equal to 6 or 12 mm. The width and length of the plate are 130 and 288 mm, respectively. The wire electrical discharge machine is presented in Fig. 3. An AC power supply is the source of power for plate type heaters. Both rear faces of the test section are insulated with a 10-mm-thick, heat-resistant Mica standard sheet, 5-mm-thick Aeroflex standard sheet, and then a 5-mm-thick Acrylic standard sheet. The temperature distribution at the top and bottom wavy walls are measured by three T-type copper-constantan thermocouples with 1-mm-diameter probes. The thermocouples were mounted on the wall (the holes were drilled on the rear face) and fixed with a special glue.

Operating Conditions. In the experiments, the rate of the air flow entering the test section was increased by small increments, while the supplied heat on both sides of the arc-shaped wavy wall was kept constant. The heat supplied to the walls was adjusted to achieve the desired level by using electric heaters. In the present experiment, the voltage and current supplied to the heaters were measured using a digital clamp meter. The temperature at each posi-

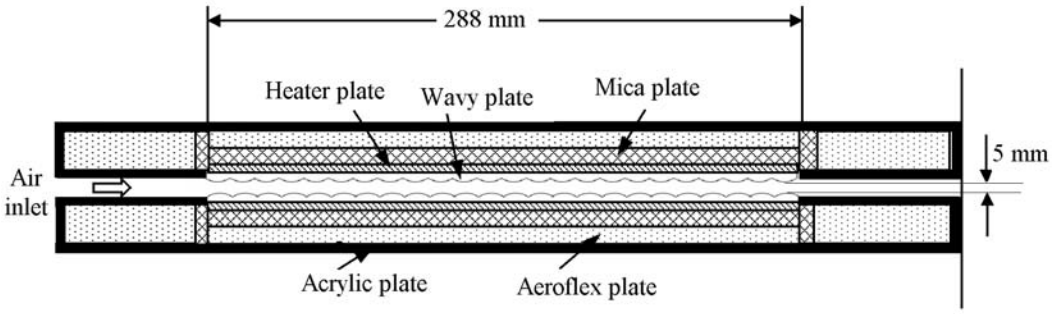

Fig. 3. Schematic diagram of the test channel.

tion and pressure drop across the test section were recorded three times. Data collection was carried out using a data acquisition system (DataTaker, DT800) having a capacity of 40 channels. The temperatures at each position and pressure drops across the test section were averaged over the time period. The accuracies of measurement of the voltage, current, and air flow rate were equal to 0.2% each.

Mathematical Modeling. For the geometry shown in Fig. 2, the k–ε standard turbulence model [22–24] is employed to simulate the turbulent heat-transfer and flow characteristics. The main governing equations can be written in the following form:

continuity equation

$$\frac{\partial \rho}{\partial t} + \operatorname{div}(\rho \mathbf{U}) = 0 ; \tag{1}$$

momentum equations

$$x\text{-momentum:} \quad \rho \frac{Du}{Dt} = -\frac{\partial p}{\partial x} + \operatorname{div}(\mu \operatorname{grad} u) + S_{Mx} , \tag{2}$$

$$y\text{-momentum:} \quad \rho \frac{Dv}{Dt} = -\frac{\partial p}{\partial y} + \operatorname{div}(\mu \operatorname{grad} v) + S_{My} ; \tag{3}$$

energy equation

$$\rho \frac{Di}{Dt} = -p \operatorname{div} \mathbf{U} + \operatorname{div}(\kappa \operatorname{grad} T) + \Phi + S ; \tag{4}$$

turbulent kinetic energy equation

$$\frac{\partial (\rho k)}{\partial t} + \operatorname{div}(\rho k \mathbf{U}) = \operatorname{div}\left(\frac{\mu_t}{\sigma_k} \operatorname{grad} k\right) + 2\mu_t E_{ij} \cdot E_{ij} - \rho\varepsilon , \tag{5}$$

turbulent kinetic energy dissipation equation

$$\frac{\partial (\rho \varepsilon)}{\partial t} + \operatorname{div}(\rho \varepsilon \mathbf{U}) = \operatorname{div}\left(\frac{\mu_t}{\sigma_\varepsilon} \operatorname{grad} \varepsilon\right) + C_{\varepsilon 1} \frac{\varepsilon}{k} \cdot 2\mu_t E_{ij} \cdot E_{ij} - C_{\varepsilon 2} \rho \frac{\varepsilon^2}{k} . \tag{6}$$

The empirical constants for the turbulence model are obtained from comprehensive data for a wide range of turbulent flows [22–24]:

$$C_\mu = 0.09 , \quad C_{\varepsilon 1} = 1.47 , \quad C_{\varepsilon 2} = 1.92 , \quad \sigma_k = 1.0 , \quad \sigma_\varepsilon = 1.3 . \tag{7}$$

Boundary Conditions. No-slip and constant heat flux boundary conditions are applied on the test section as follows:

$$u = 0\,,\ v = 0\,,\ \ q = q_{\mathrm{w}}\,. \tag{8}$$

Initial Conditions. As the inlet boundary conditions, the uniform profiles for all the properties are used:

$$u = u_{\mathrm{in}}\,,\ \ v = 0\,,\ \ T = T_{\mathrm{in}}\,,\ \ k = k_{\mathrm{in}} = \frac{3}{2}\,(u_{\mathrm{in}} I)^2\,,\ \ \varepsilon = \varepsilon_{\mathrm{in}} = C_{\mu}^{3/4}\,\frac{k^{1/2}}{L}\,. \tag{9}$$

In the present study, the turbulence characteristic length L is set to be $0.07r_{\mathrm{h}}$. The factor 0.07 is based on the maximum value of the mixing length in a fully developed turbulent flow [24]. The turbulent intensity level I is defined as the ratio of the root-mean-square of the velocity fluctuation u' to the mean flow velocity u as follows:

$$I = \frac{u'}{u}\cdot 100\%\,. \tag{10}$$

Numerical Computation. The governing equations (1)–(10) are a set of convection equations with velocity and pressure coupling. Based on the control volume method, the SIMPLEC algorithm of Van Doormal and Raithby [25] is employed. The second-order upwind scheme and structured uniform grid system are used to discretize the main governing equations. In order to obtain satisfactory solutions, the grid independence was attained in the analysis by adopting different grid distributions (80,000, 150,000, and 220,000). The grid independence test indicated that the grid system of 150,000 ensures a satisfactory solution. This is verified by the fact that the difference of the computed results for the outlet air temperature, arc-shaped wavy plate temperature, and the Nusselt number with a grid finer than 150,000 (e.g., 220,000) is within 1%. The commercial program NASTRAN/CFDsign was employed as a numerical solver. The numerical computation is ended when the residual summed over all the computational nodes satisfies the criterion of 10^{-5}.

Results and Discussion. The steady-state sensible heat gain by the air flow can be determined from an energy balance. In the present analysis, only the data that satisfy the energy-balance condition $|Q_{\mathrm{h}} - Q_{\mathrm{a}}| < 10\%$ are used. The average heat-transfer rate Q_{ave} is obtained by averaging the heat transferred to the heater and the heat removed by cooling air. To represent the results and characterize the heat transfer and flow in the channel with arc-shaped wavy plates, the following variables and parameters are introduced:

$$T_{\mathrm{a.b}} = \frac{\int_0^{A_{\mathrm{cr}}} u T_{\mathrm{a}}\, dA_{\mathrm{cr}}}{\int_0^{A_{\mathrm{cr}}} u\, dA_{\mathrm{cr}}}\,, \tag{11}$$

$$\mathrm{Nu} = \frac{\dfrac{Q_{\mathrm{ave}}}{A_{\mathrm{c}}}\, d_{\mathrm{h}}}{\kappa\,(T_{\mathrm{s.ave}} - T_{\mathrm{a.b}})}\,,\ \ T_{\mathrm{s.ave}} = \frac{1}{\bar{\sigma}}\int_0^{\bar{\sigma}} T_{\mathrm{s}x}\, dx\,, \tag{12}$$

$$\mathrm{Re} = \frac{\rho u_{\mathrm{in}} d_{\mathrm{h}}}{\mu}\,, \tag{13}$$

$$d_{\mathrm{h}} = \frac{4A_{\mathrm{cr}}}{P}\,, \tag{14}$$

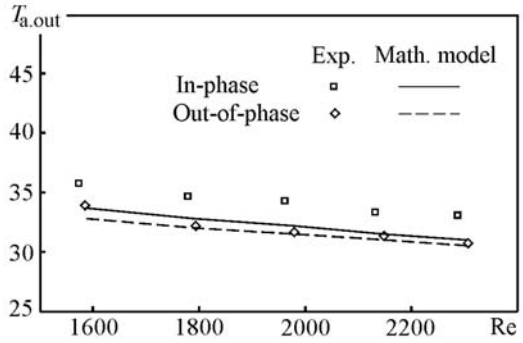

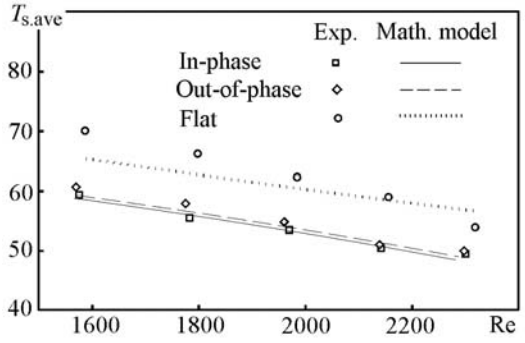

Fig. 4. Variation of the outlet air temperature with the air Reynolds number Re for 6 mm arc wavy plates at q = 0.52 kW/m^2. $T_{a.out}$, ^{o}C.

Fig. 5. Variation of the average plate temperature with Re for 12 mm arc wavy plates at q = 1.11 kW/m^2. $T_{s.ave}$, ^{o}C.

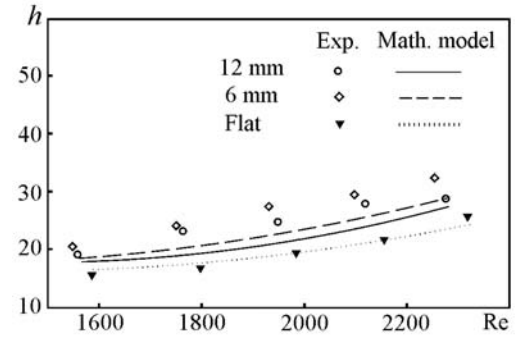

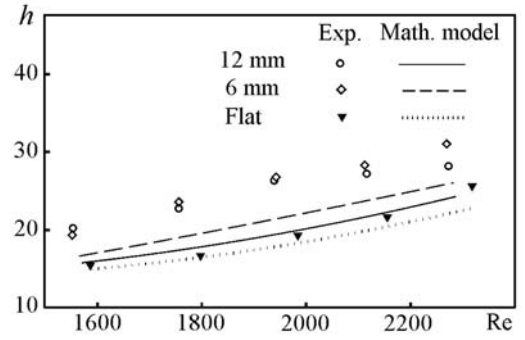

Fig. 6. Variation of the heat-transfer coefficient with Re for in-phase wavy plates at q = 1.11 kW/m^2. h, W/(m^2.^{o}C).

Fig. 7. Variation of the heat-transfer coefficient with Re for out-of-phase wavy plates at q = 1.11 kW/m^2. h, W/(m^2.^{o}C).

$$\frac{\Delta p_{ave}}{\sigma} = \frac{f_{ave}\rho u_{in}^2}{2d_h}. \qquad (15)$$

The variation of the outlet air temperature with the air Reynolds number for the 6 mm arc wavy plates with different arrangements is shown in Fig. 4. It is seen that this temperature decreases with increase in the air mass flow rate. At the same air Reynolds number, the outlet air temperatures for wavy plates with an out-of-phase arrangement are lower than those for an in-phase one. This is because the wavy plates with an in-phase arrangement have a larger effect on the recirculation flow. In addition, the results obtained from the numerical study are compared with those measured. It can be clearly seen that the predicted outlet air temperatures agree well with the measured data (the average error is 3.66%).

Figure 5 shows the variation of the average temperature for the 12 mm arc wavy plates with Re. It is seen that this temperature decreases with an increasing air mass flow rate. It can also be seen that the average temperatures for an in-phase arrangement are lower than those for an out-of-phase one. Moreover, the average plate temperature for the wavy plates is lower than that for flat plates. This is because the wavy plate has a more significant effect on the heat-transfer and flow characteristics. The predicted results are in reasonable agreement with the measured data (the average error is 2.64%).

Figures 6 and 7 show the variation of the average heat-transfer coefficient with the air Reynolds number for various wavy plate configurations. It can clearly be seen from these figures that the heat-transfer coefficient increases with the Reynolds number. For a given Re, the heat-transfer coefficients of the 6 mm arc wavy plates are higher than

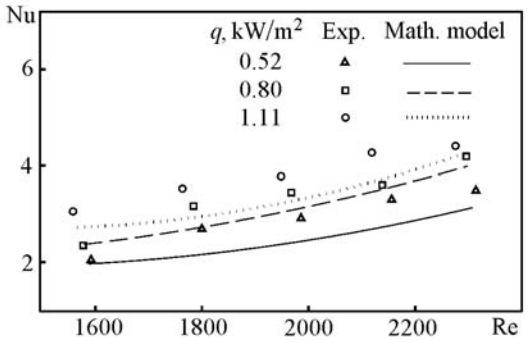

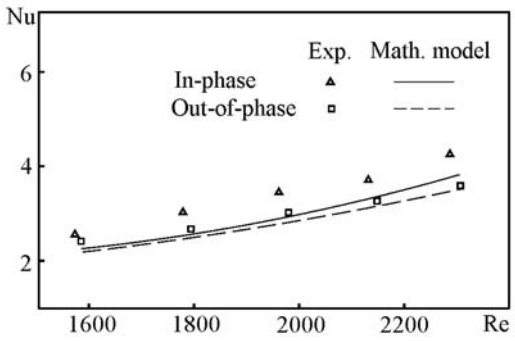

Fig. 8. Variation of the Nusselt number with Re for 12 mm arc wavy plates at different heat fluxes.

Fig. 9. Variation of the Nusselt number with Re for 6 mm arc wavy plates at q = 0.52 kW/m^2.

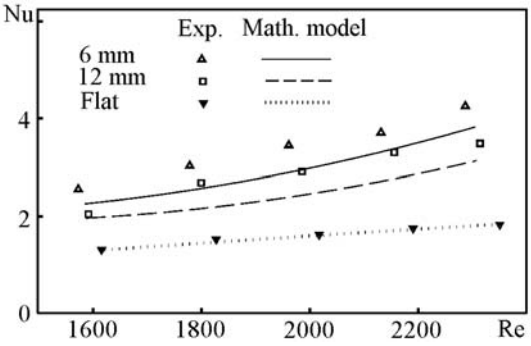

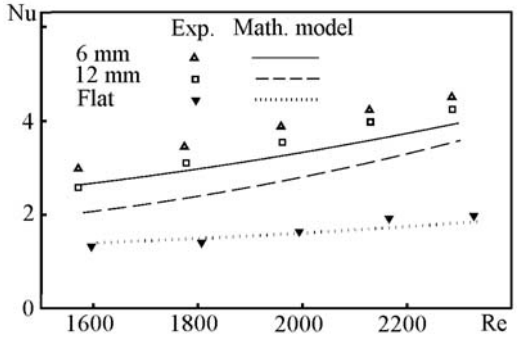

Fig. 10. Variation of the Nusselt number with Re for in-phase wavy plates at q = 0.52 kW/m^2.

Fig. 11. Variation of the Nusselt number with Re for out-of-phase wavy plates at q = 0.79 kW/m^2.

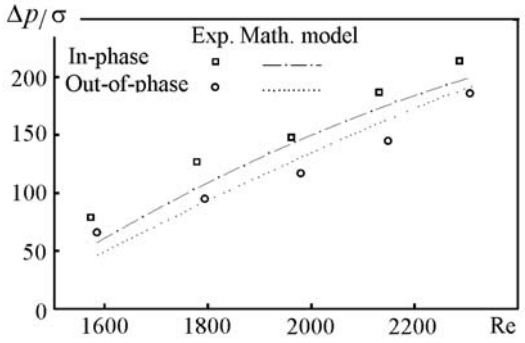

Fig. 12. Variation of the pressure drop per unit length with Re for 6 mm arc wavy plates at q = 0.52 kW/m^2. $\Delta p/\sigma$, kPa/m.

those for the 12 mm arc plates and flat ones. The reason is that the size of arc-shaped wavy plates has a significant influence on the onset and growth of the recirculation zones which promote the mixing of fluid in the thermal boundary layer, thereby enhancing convective heat transfer. The predicted results are compared with experimental data. It can be noted that the model slightly underpredicts the latter. Figures 8 and 9 show that the results obtained from the model are in reasonable agreement with those obtained experimentally.

Figures 10 and 11 show the effect of the heat flux and wavy plate arrangement on the dependence Nu(Re). As expected, the Nusselt numbers at a higher heat flux are greater than those at a lower one. Due to higher fluid re-

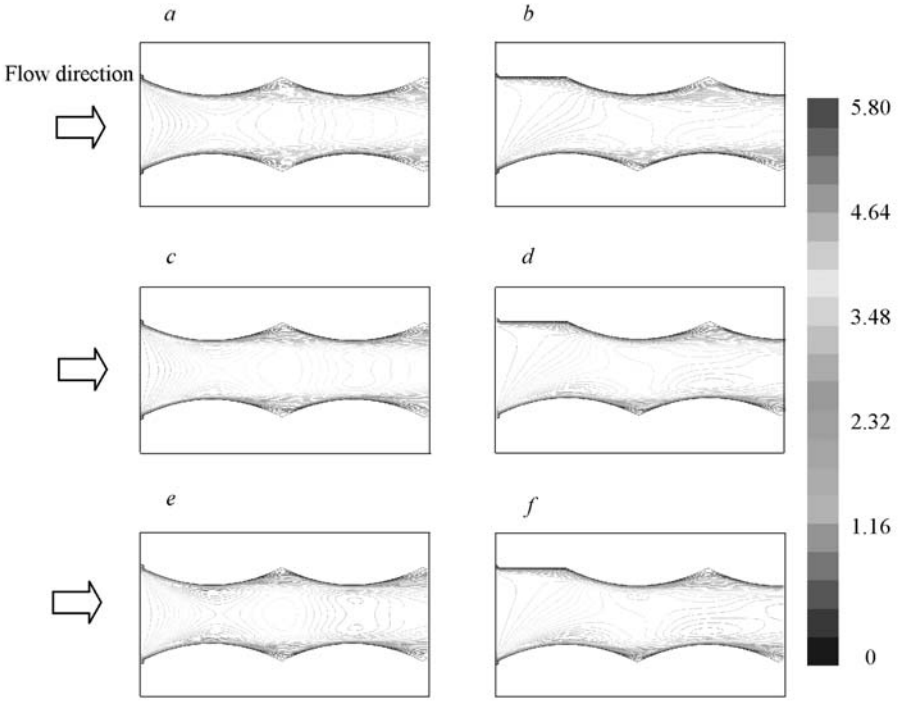

Fig. 13. Velocity contours for 6 mm arc wavy plates with in-phase (a, c, and e) and out-of-phase (b, d, and f) arrangements at different values of the mass flow rate: m = 0.002 (a and b); 0.0025 (c and d); 0.0029 kg/sec (e and f).

circulation or/and higher swirl flow intensity in the wavy troughs, the Nusselt numbers of the 6 mm arc wavy plates in an in-phase arrangement are greater than those in an out-of-phase one. There is a reasonable agreement between the results obtained from the model and experiment.

Figure 12 shows the variation of the pressure drop per unit length with the air Reynolds number for different wavy plate arrangements. In general, the pressure drop across the channel is produced by: a rotational flow formed by the wavy plate, drag forces exerted on the flow field by the wavy surface, and turbulence augmentation. It can be clearly seen that the pressure drop increases with Re. However, the rate of this increase slightly decreases as Re increases. For the given air Reynolds number, the pressure drops obtained for the channel with arc plates in an in-phase arrangement are higher than those for an out-of-phase arrangement. A reasonable agreement with experimental data is obtained.

Figure 13 gives velocity contours for the wavy plates at different mass flow rates.

Conclusions. Breaking and destabilization in a thermal boundary layer occur in a fluid flowing through a channel with wavy surfaces. Therefore, in designing a heat exchanger to increase energy saving, the use of wavy plates is a suitable method. Experimental data are employed to verify the results obtained from the model. The predicted results agree well with the measured data. The arc-shaped wavy plate configuration and arrangement have a significant effect on the enhancement of the heat transfer and pressure drop.

The author would like to express his appreciation to the Thailand Research Fund and the Srinakharinwirot University for providing financial support for this study.

NOTATION

A, flow area; $C_{\varepsilon 1}, C_{\varepsilon 2}, C_{\mu}$, turbulent-model constants; d_h, hydraulic diameter; E_{ij}, deformation-rate tensor; f, friction factor; h, heat-transfer coefficient; I, turbulent intensity; i, enthalpy; k, turbulent kinetic energy; L, turbulence characteristics length; m, mass flow rate; Nu, Nusselt number; P, wetting perimeter; p, pressure; Q, heat-transfer rate; q, heat flux; Re, air Reynolds number; r_h, hydraulic radius; S, heat source; S_{Mx}, S_{My}, sources due to mass forces; T,

temperature; t, time; **U**, velocity vector; u and v, longitudinal and normal velocity components; u', velocity fluctuation; x and y, longitudinal and normal coordinates; Δp, pressure drop; ε, dissipation kinetic energy; κ, thermal conductivity; μ, viscosity; ρ, density; σ, distance from the leading edge of the wavy plate along the wavy surface; σ_ε and σ_k, diffusion Prandtl numbers for ε and k; Φ, viscosity energy dissipation function. Subscripts: a, air; ave, average; b, bulk; c, corrugated; cr, cross section; h, heater; in, inlet; out, outlet; s, surface; t, turbulent; w, wall.

REFERENCES

1. B. Sunden and T. Skoldheden, Heat transfer and pressure drop in a new type of corrugated channels, *Int. Comm. Heat Mass Transfer*, **12**, 559–566 (1985).
2. B. Sunden and T. Skoldheden, Periodic laminar flow and heat transfer in a corrugated two-dimensional channel, *Int. Comm. Heat Mass Transfer*, **6**, 215–225 (1989).
3. D. Sawyer, M. Sen, and H. C. Chang, Heat transfer enhancement in three-dimensional corrugated channel flow, *Int. J. Heat Mass Transfer*, **41**, 3559–3573 (1998).
4. D. Bereiziat and R. Devienne, Experimental characterization of Newtonian and non-Newtonian fluid flows in corrugated channels, *Int. J. Eng. Sci.*, **37**, 1461–1479 (1999).
5. G. Fabbri, Heat transfer optimization in corrugated wall channels, *Int. J. Heat Mass Transfer*, **43**, 4299–4310 (2000).
6. G. Fabbri and R. Rossi, Analysis of the heat transfer in the entrance region of optimised corrugated wall channel, *Int. Comm. Heat Mass Transfer*, **32**, 902–912 (2005).
7. M. A. Mehrabian and R. Poulter, Hydrodynamics and thermal characteristics of corrugated channels: computational approach, *Applied Mathematical Modelling*, **24**, 343–364 (2000).
8. M. Gradeck and M. Lebouche, Two-phase gas-liquid flow in horizontal corrugated channels, *Int. J. Multiphase Flow*, **26**, 435–443 (2000).
9. M. Gradeck, B. Hoareau, and M. Lebouche, Local analysis of heat transfer inside corrugated channel, *Int. J. Heat Mass Transfer*, **48**, 1909–1915 (2005).
10. M. Vasudevaiah and K. Balamurugan, Heat transfer of rarefied gases in a corrugated microchannel, *Int. J. Thermal Science*, **40**, 454–468 (2001).
11. C. Zimmerer, P. Gschwind, G. Gaiser, and V. Kottke, Comparison of heat and mass transfer in different heat exchanger geometries with corrugated walls, *Experimental Thermal and Fluid Science*, **26**, 269–273 (2002).
12. C. C. Wang and C. K. Chen, Forced convection in a wavy-wall channel, *Int. J. Heat Mass Transfer*, **45**, 2587–2595 (2002).
13. A. Hamza, H. Ali, and Y. Hanaoka, Experimental study on laminar flow forced-convection in a channel with upper V-corrugated plate heated by radiation, *Int. J. Heat Mass Transfer*, **45**, 2107–2117 (2002).
14. H. M. Metwally and R.M. Manglik, Enhanced heat transfer due to curvature-induced lateral vortices in laminar flows in sinusoidal corrugated-plate channels, *Int. J. Heat Mass Transfer*, **47**, 2283–2292 (2004).
15. Y. Islamoglu and C. Parmaksizoglu, The effect of channel height on the enhanced heat transfer characteristics in a corrugated heat exchanger channel, *Applied Thermal Engineering*, **23**, 979–987 (2003).
16. Y. Islamoglu and A. Kurt, Heat transfer analysis using ANNs with experimental data for air flowing in corrugated channels, *Int. J. Heat Mass Transfer*, **47**, 1361–1365 (2004).
17. Y. Islamoglu and C. Parmaksizoglu, Numerical investigation of convective heat transfer and pressure drop in a corrugated heat exchanger channel, *Applied Thermal Engineering*, **24**, 141–147 (2004).
18. P. Naphon, Laminar convective heat transfer and pressure drop in the corrugated channels, *Int. Comm. Heat Mass Transfer*, **34**, 62–71 (2007).
19. P. Naphon, Heat transfer characteristics and pressure drop in the channel with V-corrugated upper and lower plates, *Energy Conversion and Management*, **48**, 1516–1524 (2007).
20. P. Naphon, Effect of corrugated plates in an in-phase arrangement on the heat transfer and flow developments, *Int. J. Heat Mass Transfer*, **51**, 3963–3971 (2008).
21. S. Kuhn and P. R. V. Rohr, Experimental investigation of mixed convective flow over a wavy wall, *Int. J. Heat Mass Transfer*, **51**, 94–106 (2008).

22. P. H. Oosthuizen and D. Nayler, *An Introduction to Convective Heat Transfer Analysis*, Mc-Graw-Hill, New York (1999).
23. B. E. Launder and D. B. Spalding, *Mathematical Models of Turbulence*, Academic Press, London (1973).
24. H. K. Versteeg and W. Malalasekera, *Computational Fluid Dynamics*, Longman Group, London (1995).
25. J. P. Van Doormal and G. D. Raithby, Enhancements of the SIMPLEC method for predicting incompressible fluid flows, *Numerical Heat Transfer*, **7**, 147–163 (1984).